Evaluating Laramide Orogenesis Via Flexural Basin Response In The San Juan Basin, New Mexico And Colorado

Kurt Rudolph, Ryan Leary, Tyson Smith, and Kristine Zellman
2025, pp. 137-152. https://doi.org/10.56577/FFC-75.137

in:

Geology of the Eastern San Juan Basin - Fall Field Conference 2025, Hobbs, Kevin M.; Mathis, Allyson; Van Der Werff, Brittney;, New Mexico Geological Society 75 th Annual Fall Field Conference Guidebook, 227 p. https://doi.org/10.56577/FFC-75

This page is intentionally left blank to maintain order of facing pages.

New Mexico Geological Society Guidebook, 75th Fall Field Conference, 2025, p. 137–151, https://doi.org/10.56577/FFC-75.137

EVALUATING LARAMIDE OROGENESIS VIA FLEXURAL BASIN RESPONSE IN THE SAN JUAN BASIN, NEW MEXICO AND COLORADO

KURT RUDOLPH[1], RYAN LEARY[2], TYSON SMITH[3], AND KRISTINE ZELLMAN[3]

[1]Rice University and University of Houston, 9 Rabbitbrush, Santa Fe, NM 87506; kwrudolph54@gmail.com
[2]New Mexico Institute of Mining and Technology, 801 Leroy Place, Socorro, NM 87801
[3]U.S. Geological Survey, Denver Federal Center, P.O. Box 25046, MS 980, Denver, CO 80225

Abstract—A challenge in interpreting the location, timing, and magnitude of ancient orogenic events is that ongoing uplift and erosion in the hinterlands often destroys much of the primary record of these events. However, basin-thickness patterns in the sedimentary record can provide complementary evidence of uplift via flexural effects. Here, we deploy well-log correlation, isochores, basin modeling, flexural modeling, and subcrop mapping to evaluate the Late Cretaceous to Paleogene basin response to Laramide tectonism in the San Juan Basin. A wedge of upper Campanian to Maastrichtian sedimentary rock thickens from 200 to 800 m from southeast to northwest in the basin. This pattern can be successfully simulated via flexural modeling if we infer early Laramide uplift along the northwest basin flank that produced a 0.8-km-high topographic load. The Laramide unconformity bounds the top of this Upper Cretaceous sedimentary wedge and truncates progressively older strata to the east, further supporting a westward tilt of the basin. The onset of Campanian Laramide flexure may have also contributed to the profound transgression from the upper Menefee Formation to the Lewis Shale. The Paleocene isochore map displays an approximately symmetrical pattern, with thickening toward the center of the basin. This suggests the possibility of competing flexural loads. The base Eocene structure indicates an asymmetric deep on the northeast flank of the basin, providing flexural evidence of contemporaneous uplift/loading of the Nacimiento uplift and Archuleta arch; this has been modeled as ~2.1-km load height. Both Cretaceous and Paleocene sedimentary wedges are narrow, suggesting low flexural rigidity; modeled effective elastic thicknesses (EET) are 20–30 km, comparable to estimates of modern EET for the region.

INTRODUCTION

The interplay of tectonics and sedimentary basin evolution is a long-standing subject of research. Of particular interest is the effect of flexural loading in contractional systems as a driver of subsidence and sedimentary accommodation (Beaumont, 1981). This is the origin of foreland basins, which are formed due to the progressive loading by the adjacent orogenic wedge (DeCelles and Giles, 1996). Moreover, the rising hinterlands are commonly an important source of the sediments that fill the basins.

In areas where thick-skinned tectonism has partitioned a region into basins and uplifts, the same mechanisms are operative; however, subsidence and sedimentation patterns can be more complex because of high variability in the timing and location of the uplifts and resulting flexure. Two North American examples of thick-skinned intraplate systems that exhibit these complex flexural patterns are the Ancestral Rocky Mountain (Kluth, 1986; Leary et al., 2017; Rudolph, 2023) and Laramide orogenies (e.g., Dickinson et al., 1988; Weil and Yonkee, 2023).

A particular challenge in these intraplate systems is that ongoing uplift and exhumation of the structural highs usually destroys direct evidence of the early location and magnitude of the uplifts. However, the response of sedimentary basins, in terms of subsidence and paleogeography, provides an alternative window into these systems.

In this study, we evaluate the Late Cretaceous through Eocene tectonic history of the San Juan Basin of New Mexico and Colorado by examining basin subsidence using an approach similar to that of Hagen et al. (1985) and Saylor et al. (2020).

GEOLOGIC SETTING

The Western Interior Seaway of North America was a foreland basin associated with retroarc thrusting of the Sevier orogeny (Supplement 1.1). The orogenic front was active between 155 and 55 Ma (DeCelles, 2004), during which time the resultant Sevier continuous foreland basin transitioned into a series of broken foreland basins, partitioned by local basement uplifts (Yonkee and Weil, 2015; Horton et al., 2022; Weil and Yonkee, 2023). In Coniacian-Santonian time, the system evolved from a simple flexural foreland to a basin with long-wavelength dynamic subsidence that has been attributed to the interactions with the downgoing Farallon plate, including mantle flow (Liu and Nummedal, 2004; Liu and Gurnis, 2010). By Maastrichtian time, basement-involved uplifts fragmented the precursor basin into a mosaic of uplifts and basins, partitioning the seaway (e.g., Coney, 1971; Chapin and Cather, 1983; Dickinson et al., 1988; Weil and Yonkee, 2012; Copeland et al., 2017). Termed the Laramide orogeny, east-northeast-directed deformation extended to southern Montana and southward to New Mexico (e.g., Dickinson et al., 1988). Laramide orogenesis was caused by a change to flat-slab subduction of the Farallon plate, which terminated in the middle to late Eocene (Yonkee and Weil, 2015; Weil and Yonkee, 2023). Following the Laramide orogeny, slab-rollback resulted in extensive calc-alkalic volcanism across the region in the late Eocene through Oligocene (e.g., Lipman et al., 1972; McIntosh et al., 1992).

The San Juan Basin of northwestern New Mexico and southwestern Colorado is in the southern portion of the Laramide province and is one of 15–20 similar Laramide basins

(Dickinson et al., 1988; Supplement 1.1). The San Juan Basin is approximately equidimensional and has steeply dipping flanks on the west, north, and east sides, associated with the Hogback monocline/Defiance uplift, Archuleta arch/San Juan uplift, and Nacimiento uplift, respectively (Fig. 1; Baltz, 1967; Fassett, 1991). The basin's southern flank is gentler and rises gradually onto the Zuni uplift (Cather, 2003, 2004).

The San Juan Basin contains up to 4 km of Paleozoic to Cenozoic sedimentary rocks. The focus of this study is the upper 2 km that consist of Upper Cretaceous through Eocene strata (Fig. 2). Upper Cretaceous strata consist of cyclic offshore to nearshore marine/coastal plain siliciclastic rock. At a second-order (>10 My) scale, three retrogradational-progradational packages are recognized, which are best delimited by maximum flooding surfaces in the lower Mancos Shale, Greenhorn Limestone Member, upper Mancos Shale, and Lewis Shale (Fig. 2). Upper Cretaceous sediments prograded to the north-northeast, with shorelines that were oriented east-southeast to west-northwest (Supplement 1.5). Maastrichtian rocks (Fruitland Formation and Kirtland Formation) were deposited in entirely nonmarine coastal plain and fluvial environments. Like other Laramide basins, there is an unconformity at the top of the Cretaceous, termed the Laramide unconformity. From biostratigraphic and dated ash-bed control, a lacuna of approximately 7–8 My is interpreted at this surface (Fassett, 2000). A basal Paleocene fluvial conglomeratic sandstone rests on this surface in most of the basin (Ojo Alamo Sandstone). The overlying nonmarine Nacimiento Formation (Paleocene) and San Jose Formation (lower Eocene) are only preserved in the basin axis, and have experienced significant erosion (Cather et al., 2008; Cather, at al., 2019).

METHODS

This study leveraged the vast published literature as well as the public domain well data available through the New Mexico

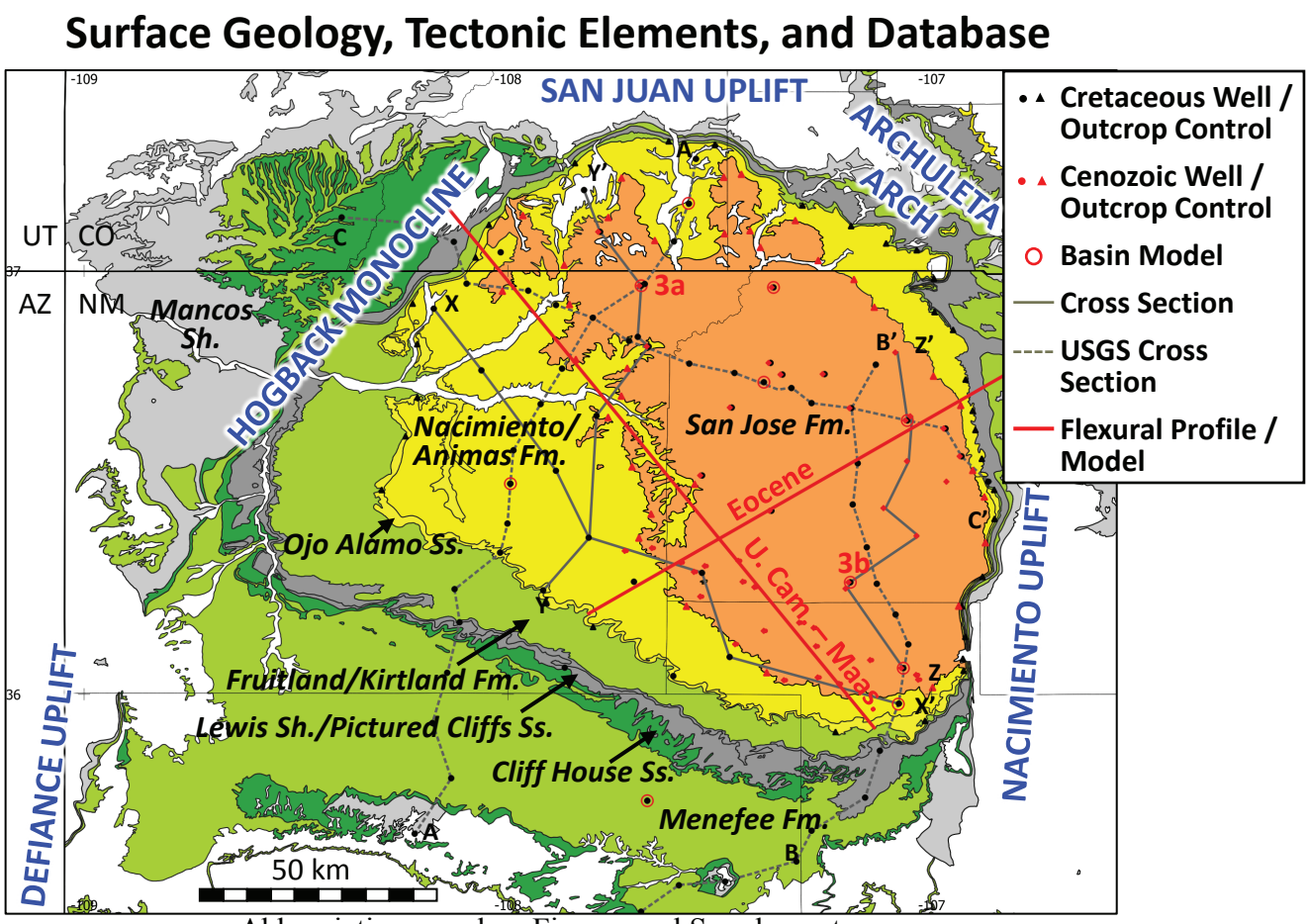

Abbreviations used on Figures and Supplements

Fm.	Formation	Ls.	Limestone	Eoc.	Eocene	Con.	Coniacian
Mbr.	Member	MFS	Maximum Flooding Surface	Pal.	Paleocene	Tur.	Turonian
Sh.	Shale	FS	Flooding Surface	Maa.	Maastrichtian	Cen.	Cenomanian
Ss.	Sandstone	C.I.	Contour Interval	Cam.	Campanian	U.	Upper

Figure 1. Surface geology of the San Juan Basin with key data control and analyses used in this study, and major tectonic elements. Shapefiles used to generate this map are from Horton (2017). The three U.S. Geological Survey (USGS) cross sections are from Molenaar and Baird (1992). Additional well logs, including cross sections X–X' and Y–Y', were correlated into this framework. Regional setting and location of study area is depicted in Supplement 1.1.

(New Mexico Energy Minerals and Natural Resources Department, 2025) and Colorado (Colorado Energy and Carbon Management Commission, 2025) state websites. Primary methods included well-log-based stratigraphic correlation, structure and isochore mapping, basin modeling, and flexural modeling.

Stratigraphic Framework

The regional stratigraphic cross sections of Molenaar and Baird (1992) were used as a basis for well-log correlations in Cretaceous strata, as well as the Ojo Alamo Sandstone (Fig. 1). The age control for burial models (Figs. 3A and 3B) was based on the chronostratigraphy of Molenaar (1977), and the biostratigraphy (ammonites and inoceramids) of Merewether and McKinney (2015), augmented by radiometric dating of ash beds (Fassett, et al., 1997; Fassett, 2000). This information was calibrated to the geologic time scale of Gradstein et al. (2020), as implemented in their program Time Scale Creator 8.0. Two additional cross sections were constructed (Fig. 4; Supplement

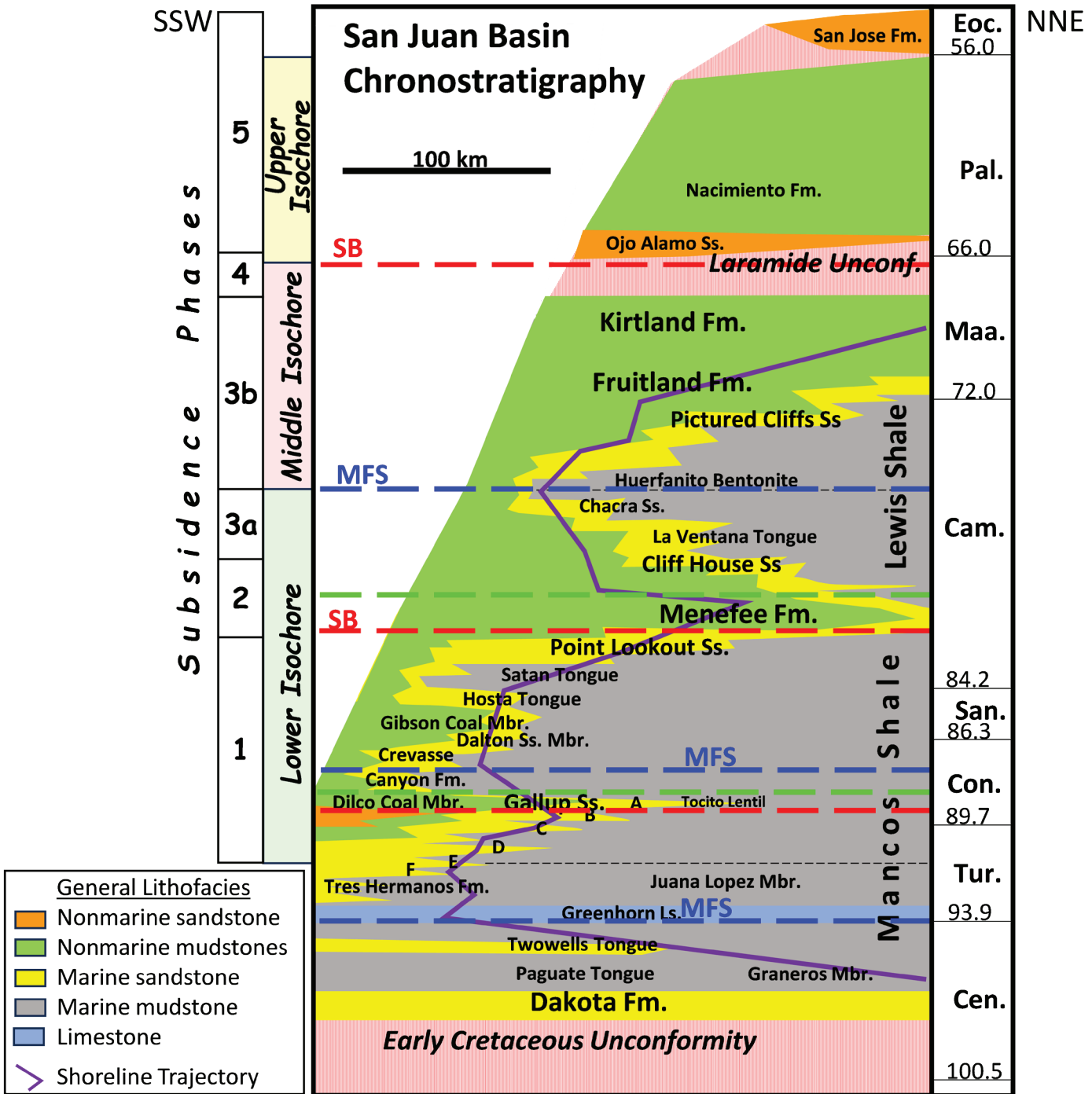

Figure 2. Chronostratigraphy of the Upper Cretaceous to lower Eocene of the San Juan Basin. A quantitative estimate of shoreline trajectories is indicated by the purple line. Large-scale cyclicity (2nd order scale) is indicated by three maximum flooding surfaces ("MFS") and sequence boundaries ("SB"). Modified from Molenaar (1977). The first five subsidence phases of Figures 3A and 3B, and the three isochore intervals of Figures 4, 5A, 5B, and 5D are indicated.

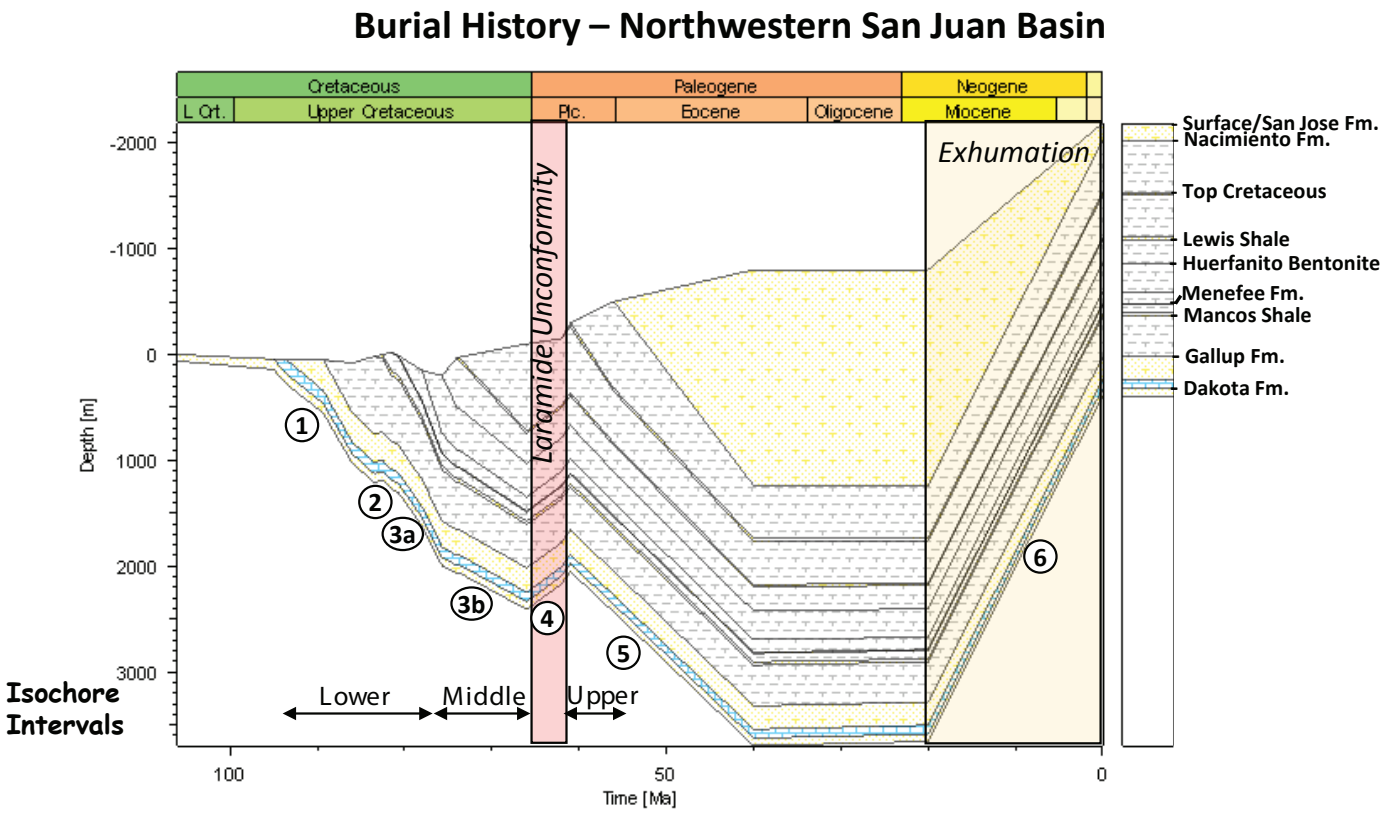

Figure 3A. Total subsidence for well 30-045-20487 in the northwestern San Juan Basin. The Laramide unconformity, extrapolated period of Cenozoic exhumation, and three isochore intervals are indicated. The six phases of Late Cretaceous subsidence/uplift (numbered) are described in the text. Location of this model is on Figure 1.

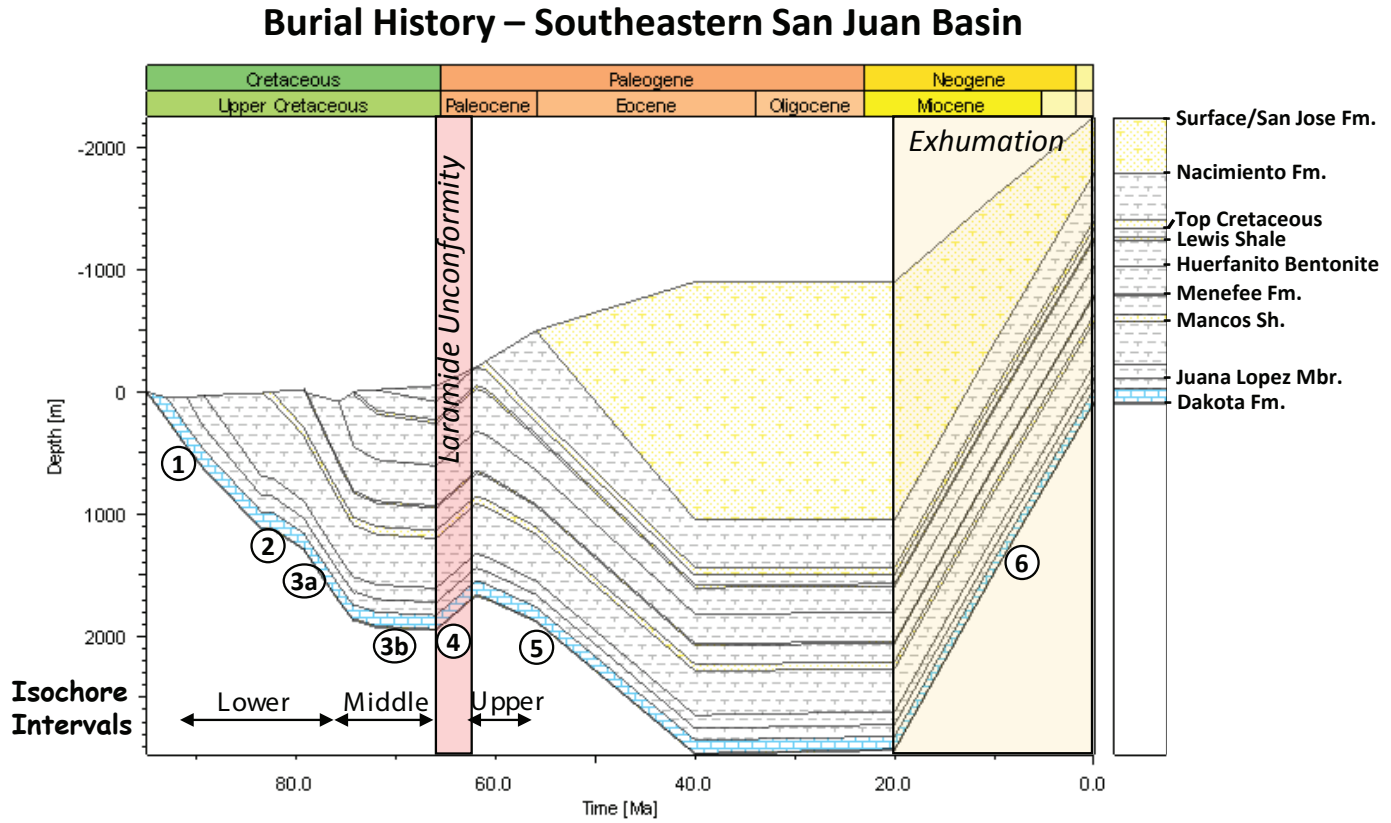

Figure 3B. Total subsidence for well 30-039-21831 in the southeastern San Juan Basin. See Figure 3A caption for description.

1.3) along with selected additional wells. For interpreting the Nacimiento Formation top, the cross section in Williamson and Lucas (1992) in the south part of the basin served as a reference, as well as cross section C-C' in Molenaar and Baird (1992). A north–south cross section was constructed for this interval (Supplement 1.4).

Four key horizons were mapped into structure maps and isochores. From oldest to youngest, these are the Juana Lopez Formation top, the Huerfanito Bentonite top, the Cretaceous/Laramide unconformity top, and the Nacimiento Formation top.

Some of these maps have been made by previous workers, most notably Fassett (2000), Cather (2003), and Cather (2004). When available, this previous work is of higher fidelity than the screening-level mapping herein, as they employ many more correlated wells. However, we have chosen to include and analyze the maps in this study to ensure consistency among maps, basin models, and flexural models. The maps within have been compared to the available published maps and found to be consistent in all cases.

Many Upper Cretaceous formations are defined lithostratigraphically and are diachronous as they reflect lateral migration of depositional facies through time as is indicated on chronstratigraphic charts (e.g., Molenaar, 1977; Fig. 2). On the cross sections (Fig. 4; Supplement 1.3), these are indicated by dashed lines. The lower three horizons used to construct isochores are meaningful with respect to chronostratigraphy, as they are a marine flooding surface (Juana Lopez Member top), an ash layer/maximum flooding surface (Huerfanito Bentonite top), and an unconformity (Cretaceous unconformity top). The

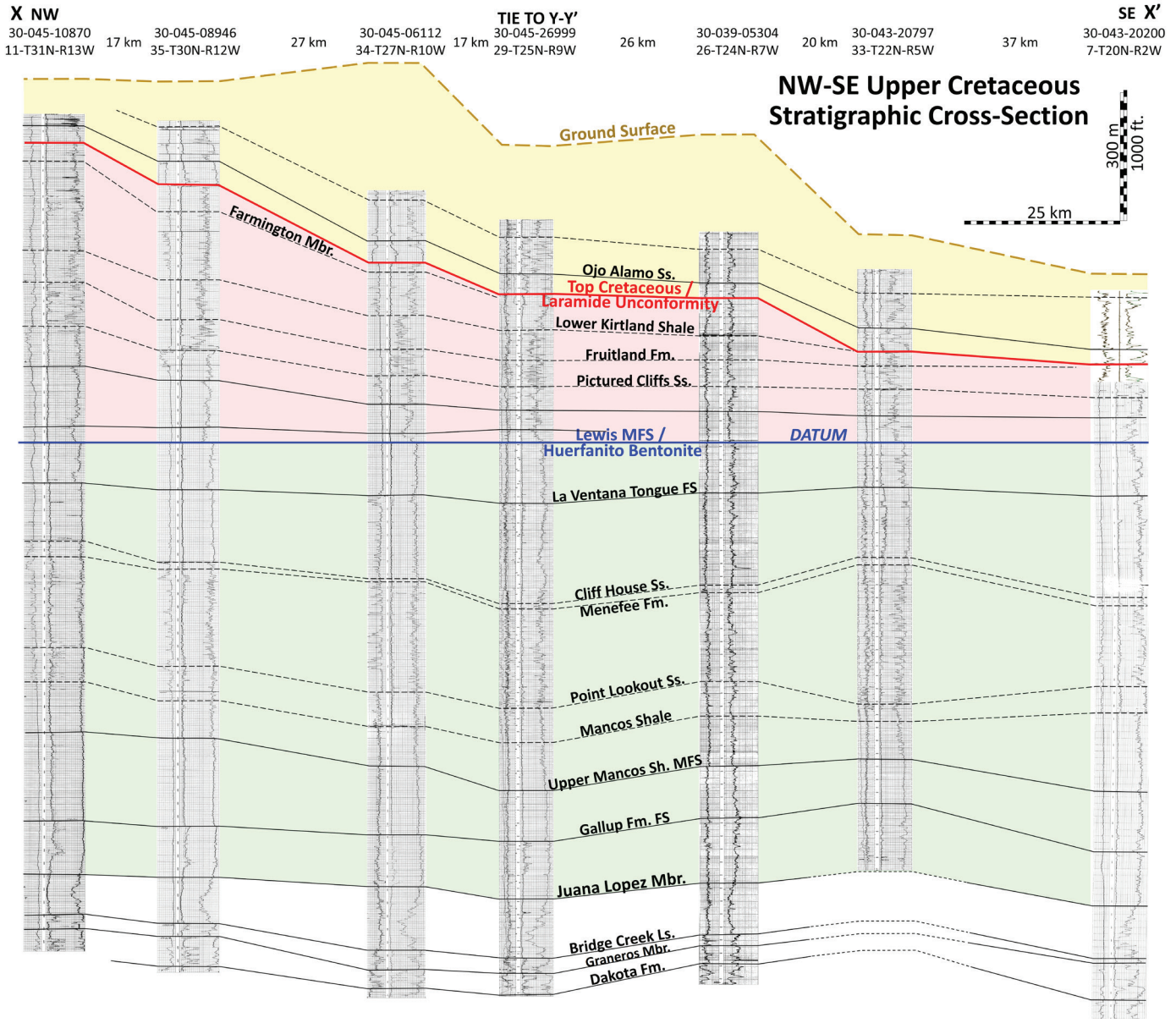

Figure 4. Stratigraphic cross section X–X'. The Juana Lopez Member to Huerfanito Bentonite interval (green) is approximately uniform. The Huerfanito Bentonite to top Cretaceous interval (red) thickens to the northwest. The Paleocene interval (yellow) is eroded along this profile, and thickness variations are not relevant. Location of the cross section is indicated on Figure 1.

Nacimiento Formation top is a difficult correlation and may suffer from greater uncertainty. The formation contact is usually marked by an increase in sandstone content and has been interpreted as unconformable, except in the northern part of the basin (Cather et al., 2019). However, recent outcrop work interpreted the surface as largely conformable and related to climatically driven fluvial progradation (Zellman et al., 2024). This difficulty and uncertainty in the Nacimiento Formation top contact is primarily due to the variable lithologic character and spatial variability of a possible unconformity.

The structure maps at the Cretaceous unconformity top and Nacimiento Formation top were extended by using the elevation of the corresponding mapped formation contact; this was accomplished by overlaying a U.S. Geological Survey digital elevation model (U.S. Geological Survey, 2021) on the U.S. Geological Survey geologic map shapefile (Horton, 2017) in QGIS.

Basin Models

The Schlumberger application PetroMod© was used to construct one dimensional (well) basin models in the San Juan Basin. The primary inputs were the depths, geologic age, and lithology of the stratigraphic horizons. At each surface, paleobathymetry/paleoelevation, basal heat flow, and paleosurface temperature must also be defined. The program decompacts (a.k.a. backstrips; Watts and Ryan, 1976) the input stratigraphic section, layer by layer, to the oldest horizon. The effect of both sediment and water load are included in the calculations. Erosion of sedimentary section can also be specified, whether it is associated with ancient unconformities or Neogene exhumation. Reconstructing missing stratigraphic section (age, thickness, and lithology) was a challenge, as the youngest preserved strata in the San Juan Basin are of early Eocene age. In this study, we calibrated additional Paleocene–Eocene burial by calibrating basin models to wellbore temperatures and published vitrinite reflectance data (Russell, 1979; Fassett and Nucio, 1990; Law, 1990; Pawlewicz et al., 1991; Broadhead et al., 1998; and Fassett, 2000).

Three families of products were generated from these 1D basin models: depth plots, time plots, and burial history plots. The parameters of temperature, vitrinite reflectance, porosity, pressure, and thermal conductivity can be displayed in any of these domains. Herein, we have only illustrated the burial history, but basin model inputs and calibrations are included in the Supplement 2. Two 1D models were previously published in the San Juan Basin by Law (1992). A total of nine models were constructed in this study.

There were two complimentary objectives of basin models. The first was to quantitatively evaluate the subsidence history. The second was to analyze and predict key parameters over geologic time and depth, especially petroleum source rock maturation. The latter application required a good understanding of the heat flow history. To test and refine the assumptions on heat flow and burial history, calibrations of model outputs against observed present-day temperature and vitrinite reflectance versus depth are important if questions of temperature and/or exhumation history are of interest (Hantschel and Kauerauf, 2009).

As the objective of this analysis was to comprehend the subsidence history, heat flow was usually not as important and only a few calibrations were completed. However, in cases where a significant amount of the section of interest has been removed by recent erosion, calibration became critical. In this study, basal heat flow has been interpreted as constant from Cretaceous to present, and the regional U.S. heat flow map developed by Blackwell et al. (2011) served as an initial estimate. Each site was refined using well temperatures (Horner- or Waples-corrected bottom hole temperatures, and temperature logs from production tests). Inputs and outputs are documented in Supplement 2.

Flexural Modeling Approach

Two flexural models for the San Juan Basin were constructed, based on the upper Campanian-Maastrichtian isochore (Huerfanito Bentonite to top Cretaceous; Fig. 5B) and the top Paleocene structure map (Nacimiento Formation; Fig. 5E). The primary inputs were stratigraphic thickness or depth control points with their position relative to the front of the load. Additional model parameters included the uncertainty range of stratigraphic thickness, range of load density, load-front position, load width and height, taper direction and maximum slope angle, range of effective elastic thickness (EET), and range of load and sediment fill densities. The software used was the MATLAB© code, FlexMC (Saylor et al., 2017), the algorithm of which uses equations from Wangen (2010). The simulation used the Monte Carlo method, and a minimum of 100,000 trials were run. Only the trials that fit the stratigraphic control points within the specified uncertainty range (thickness) were tabulated. From the subset of successful trials, the means and standard deviations are reported. Thus, few assumptions were made on the flexural controls, and the results were observationally driven. The most important parameters estimated from modeling are load height, topographic height, load width, slope, and EET. The flexural modeling program employs a simple decompaction of thicknesses for inputs not already decompacted via backstripping,

Effective elastic thickness is one of the principal controls on basin shape and subsidence pattern. Effective elastic thickness is a measure of the flexural strength of the coupled lithosphere. High EET yields a broad, shallow flexural basin, whereas low EET yields a narrow, deep foreland for the equivalent load (Beaumont, 1981).

Flexural Modeling Uncertainties

Stratigraphic inputs contain two main sources of uncertainty. First, removal of stratigraphic section at the top of the sedimentary wedge by erosion will modify the shape of the profile, especially if this erosion is not uniform. Second, stratigraphic thickness will not be entirely a function of subsidence if there are changes in paleobathymetry or paleoelevation from formation base to top. The Laramide unconformity is

the upper bounding surface for the upper Campanian to top of Cretaceous stratal interval (Fig. 2). Therefore, to flexurally model this sedimentary wedge appropriately, the removed stratigraphic interval must be reconstructed by utilizing contextual geologic information. Mapping of the subcrop indicates a progressive loss of stratigraphic section from northwest to southeast (Fig. 5C). We have estimated the differential erosion by projecting preserved thicknesses from stratigraphic cross sections, and the resulting estimates ranged from 0 to 100 m from northwest to southeast (Supplement 3). The base of this stratigraphic interval is the Huerfanito Bentonite, which lies within the distal offshore Lewis Shale, and the original top is the entirely nonmarine Kirtland Formation. Therefore, paleobathymetry/paleoelevation was variable and uncertain, and we applied an estimate of 150-m change from base to top of the stratigraphic interval. Furthermore, the modeled flexural profile is parallel to shoreline trends (Supplement 1.5), thus a uniform correction is reasonable.

Throughout the modeling, a base or reference case was described that represented our best estimate of with respect to assumptions and corrections. In addition, sensitivities to the reference case have also been modeled to evaluate uncertainty.

For the Eocene flexural profile, there were greater uncertainties. The interval is deeply eroded and estimates of exhumation from calibrated basin models ranged between 1,200 and 2,200 m (Figs. 3A and 3B; Supplement 3). This is broadly consistent with the analysis of Cather et al. (2008). However, the fidelity and density of the basin model calibrations are insufficient to reconstruct a reliable reconstructed isopach map of Eocene strata in the San Juan Basin. Therefore, the current structure map on the Nacimiento Formation top or the Eocene base (Fig. 5E) was used as the reference case for flexural modeling. This approach required two assumptions. First, the base of Eocene has not been significantly deformed (e.g., tilted) post-Eocene. Second, we can use a constant elevation datum to account for aggradation of nonmarine sediments in the semienclosed basin.

The question of how much vertical aggradation occurred in the Paleocene–Eocene is poorly constrained, but insights can be garnered from Laramide basins to the north. Given that large lacustrine systems existed in the Paleocene (Wind River basin) and the Eocene (Green River, Uinta, and Piceance basins), these systems had a semienclosed architecture in terms of basin fill (e.g., Bradley, 1948). Moreover, clumped isotope data from calcitic elements suggest that the Green River basin had an elevation of 500–1,500 m in the Paleocene-Eocene (Gao and Fan, 2018; Zhu et al., 2018). Therefore, we posit that a similar situation occurred in the San Juan Basin for the late Paleocene to Eocene, which had a more overfilled character with external (exorheic) drainage (Cather et al., 2012).

The other major uncertainty was the position of the orogenic load. The reference case assumed a front "pin," with the location of the loads consistent with the Hogback-San Juan uplift trend (late Campanian-Maastrichtian) and the Nacimiento uplift-Archuleta arch (early Eocene), respectively.

The possibility of a "far field" load, associated with the Sevier orogenic wedge has been considered very unlikely. The youngest Sevier deformation front is about 450 km to the west (Supplement 1.1). To test this, the load was conservatively assumed to be 300 km farther to the west. To yield the flexure observed in the basin from this load position, an EET of about 140 km was necessary, compared with the 20–30 km observed present day (Tesauro, 2014) and in the Late Cretaceous to Eocene (Saylor et al., 2020). More dramatically, a load height of about 15 km (!) was required (Supplement 3). For the Sevier orogeny, this analysis supported that the San Juan Basin was in a backbulge position with respect to the cordilleran orogenic wedge.

The Zuni uplift about 150 km to the south may have influenced basin sedimentation by serving as a source area. However, its possible influence as a primary load is inconsistent with the documented geometries of the Upper Cretaceous (thickens to northwest) and Eocene (thickens to east). It may have acted as a secondary load, but lack of proximity to the basin, combined with a weak coupled lithosphere, implies modest effects.

Due to the uncertainties and assumptions in the flexural model inputs described above, we performed sensitivity testing of model results, which challenged reference case assumptions (Supplement 2). For both the Eocene and Upper Cretaceous, different input profiles were tested. The Upper Cretaceous reference case assumed that uplift of the Hogback monocline was the load, and the load was pinned at its front. However, because this is a relatively low relief feature, a suite of models with variable load positions (back pin) were also tested. Broken and infinite plate models were also evaluated for both the Upper Cretaceous and Eocene yielding broadly similar results. Results of these sensitivities are documented in Supplement 3.

RESULTS AND DISCUSSION

Turonian to Late Campanian

The interval from the Juana Lopez Member top to Huerfanito Bentonite (~91.1–75.76 Ma; Fig. 2) is relatively uniform in thickness, with no asymmetry across the San Juan Basin (Figs. 4 and 5A). This is generally consistent with regional analyses of the Western Interior basin, where this is interpreted to record long-wavelength subsidence related to dynamic processes associated with mantle flow (Liu and Gurnis, 2010; Li and Aschoff, 2022). As such, there is no strong evidence of proximal basin flexural effects related to loading by adjacent Laramide uplifts and associated subsidence.

Shoreline trajectories (Fig. 1; Helland-Hansen and Martinsen, 1996), paleogeographic shorelines (Supplement 1.5), and paleocurrent data (Fig. 5A) indicate that progradation of the basin fill occurred from southwest to northeast. This was likely related to regional sediment supply, implying provenance from a Cretaceous highland to the southwest, likely in the area of the Zuni-Defiance uplift, which is a long-lived highland. Based on thermochronology, the uplift experienced several periods of exhumation, including late Neoproterozoic (~600 Ma), Ancestral Rocky Mountain (320–250 Ma), Laramide (70–40 Ma), and Colorado Plateau (25–0 Ma) uplifts (Flowers et al., 2008; Thacker, et al., 2021; Davis et al., 2022).

Late Campanian to Top Cretaceous

The interval from the Huerfanito Bentonite to the top of Cretaceous stratigraphic section (~75.76–66 Ma; Fig. 2) dramatically thickens from the southeast to the northwest, from less than 200 to 800 m (Fig. 5B). This is indicative of differential subsidence, potentially related to load-induced flexure. The flexural model corroborates that this is reasonable—the reference case scenario indicated an uplift of about 0.8 km; a location associated with the Hogback monocline and a southern extension of the San Juan uplift was interpreted (Fig. 6A). This modest relief is consistent with the current structural elevation of the area resulting from lower Mancos Shale outcrops on the high side of the monocline.

Similar observations of thickness have been made by Cather (2004) and have been attributed to Laramide load-related subsidence. This study provided further support and quantification of this interpretation.

The mean estimate of EET from the modeling was 31.3 km ($\sigma = \pm 1.5$ km) and was broadly consistent with modern estimates from seismic tomography in the area (Tesauro et al., 2014; Tesauro et al., 2015) and a previous analysis of the Upper Cretaceous by Saylor et al. (2020). Chapman and DeCelles (2021) evaluated the flexural strength of the Mogollon rift shoulder based on modeling Jurassic rifting in the area; they developed an estimate of 55 km ($\sigma = \pm 5$ km), significantly thicker. However, Saylor et al. (2020) documented a weakening of the lithosphere from Cenomanian–Turonian to the Late Cretaceous–Eocene, with the EET decreasing some 20–50 km.

Thin EET, which occurs throughout the Laramide province, explains the relatively short wavelength of these flexural basins. The position of the forebulge would be about 200 km from the load, based on flexural models of the wedge (Figs. 6A and 6B). By comparison, the Cretaceous forebulge in the Western Canada basin occurs at about 500 km from the load, with an associated EET of 100–150 km (Saylor et al., 2020). The relative weakness of the coupled lithosphere in the U.S. portion of the Western Interior basin has been attributed to bulldozing and hydration of the North American plate (i.e., the upper plate) by Farallon flat-slab subduction (Saylor et al., 2020). In contrast, the Western Canada basin did not experience Laramide orogenesis and is characterized by a broad foreland and high EET (~100 km; Saylor et al., 2020).

Limited published paleocurrent data from the Kirtland Formation (Pecha et al., 2018) indicate paleoflow to the east-northeast (strike transport, relative to flexural accommodation). This is not unusual—sediment transport more often reflects regional sediment supply considerations rather than local provenance. Longitudinal transport, parallel to the uplift, is common in flexural basins; examples include the Colville trough of North Alaska (Houseknecht, 2019), the west Green River basin of Wyoming (Dubois et al., 2004), and the Late Cretaceous Sevier foreland of Wyoming (Feldman et al., 2014).

Additionally, there was an evolution in sediment provenance, as indicated by detrital zircon analysis (Pecha et al., 2018). The Pictured Cliffs Sandstone and Fruitland Formation were sourced from the Mogollon highlands of southern New Mexico and Arizona. But the younger strata (Kirtland Formation to the San Jose Formation), display provenance from local uplifts, indicating the increasing effects of continued Laramide tectonism.

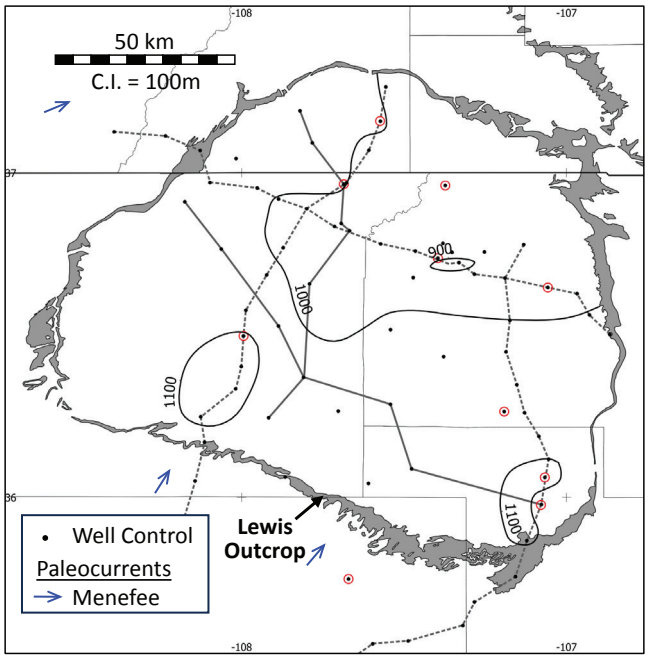

Figure 5A. Isochore of the Juana Lopez Member top to Huerfanito Bentonite interval (~91.1—75.76 Ma). Paleocurrents are generalized from the compilation of Pecha et al. (2018). This interval is relatively uniform thickness in the basin.

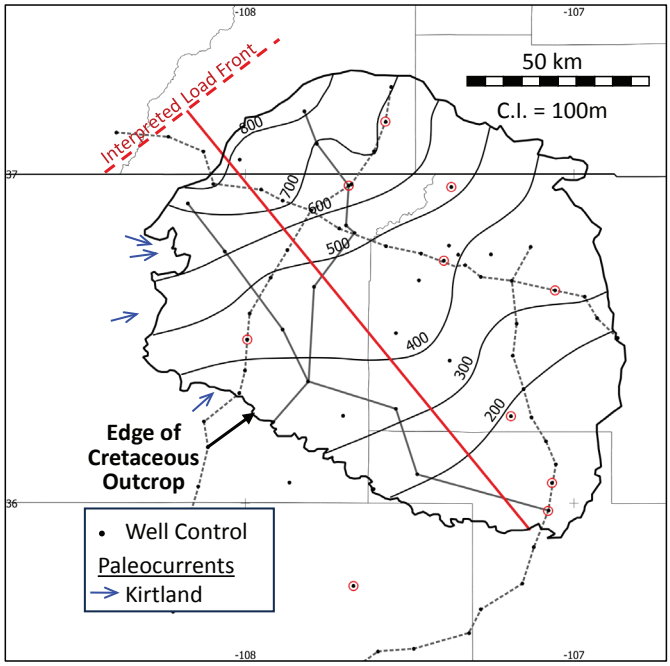

Figure 5B. Isochore of the Huerfanito Bentonite to top Cretaceous interval (~75.76–66 Ma). Paleocurrents are generalized from the compilation of Pecha et al. (2018). Thickening to the northwest is apparent. Results are very similar to Cather (2004).

Importantly, whereas there was some variability in results when different load and profile scenarios were tested (Supplement 3), all were consistent with flexure related to a contemporaneous uplift to the northwest.

Paleocene

The Paleocene stratigraphy of the San Juan Basin (Ojo Alamo Sandstone and Nacimiento Formation, ~66–55 Ma; Fig. 2) is preserved in a limited area. The associated isochore map displays a gradual thickening into the center of the basin and subtle thickening to the east (Fig. 5D). Published paleocurrent data indicate paleoflow to the southeast, perhaps indicating continued transport from the San Juan uplift/Hogback monocline, which was interpreted as emergent in the Late Cretaceous. The basal Ojo Alamo Sandstone is relatively uniform in thickness and represents a brief period of low subsidence following the Laramide unconformity. The basinward thickening is therefore accommodated within the younger Nacimiento Formation alone. We interpreted this pattern to be the result of two possible contributing factors. First, the basinward thickening toward the center of the basin, from 300 to 600 m, may represent aggradational accumulation of continental deposits in a nonmarine setting, filling antecedent topographic relief on the basin margins. Clumped isotopic analyses of Laramide basins to the north indicate paleoelevations of 500–1,500 m for the late Paleocene to Eocene (Gao and Fan, 2018; Zhu et al., 2018), indicating significant vertical aggradation. Second, this stratal thickness pattern may be evidence of uplift on the periphery of the basin, especially to the east, northeast, and northwest, resulting in a complex pattern of rimming exhumation and three-dimensional flexural effects. However, the ambiguous stratal thickness pattern and the complication of multiple possible contributing factors yielded no definitive interpretation that we provide in this paper.

Eocene

The Eocene San Jose Formation is likely deeply eroded and is preserved over a limited area. Calibrated basin models indicate 1,200–2,200 m of exhumation (Supplement 3). However, a reliable restoration via basin modeling was elusive due to the high variability of heat flow and quality of the maturity (vitrinite reflectance) calibrations. Given these constraints, the structure map at the base of the San Jose Formation (i.e., Nacimiento Formation top; Fig. 5E), was used to represent the shape of the original Eocene basin. The base of the San Jose Formation structure map shows a deep, asymmetric morphology, with a structural trough on the northeastern flank of the basin, directly adjacent to the Nacimiento uplift and Archuleta arch. Flexural models generated from reconstructed San Jose Formation stratal thickness patterns imply a mean of about 2.1 km of uplift on the Nacimiento uplift (Fig. 6B). The predicted high relief is consistent with exposure of Proterozoic granitoid rocks along the uplift. The mean EET from flexural modeling is 28.1 km ($\sigma = \pm 1.8$ km).

However, given the high uncertainty on the model inputs related to subsequent erosion, there is a range of possible load heights, with scenarios ranging from 0.7 to 3.5 km (Supplement 3). In the face of this uncertainty, the flexural nature of the Eocene San Juan Basin remains plausible as all scenarios can be successfully modeled with reasonable parameters.

Kelley et al. (1992) used apatite fission track (AFT)

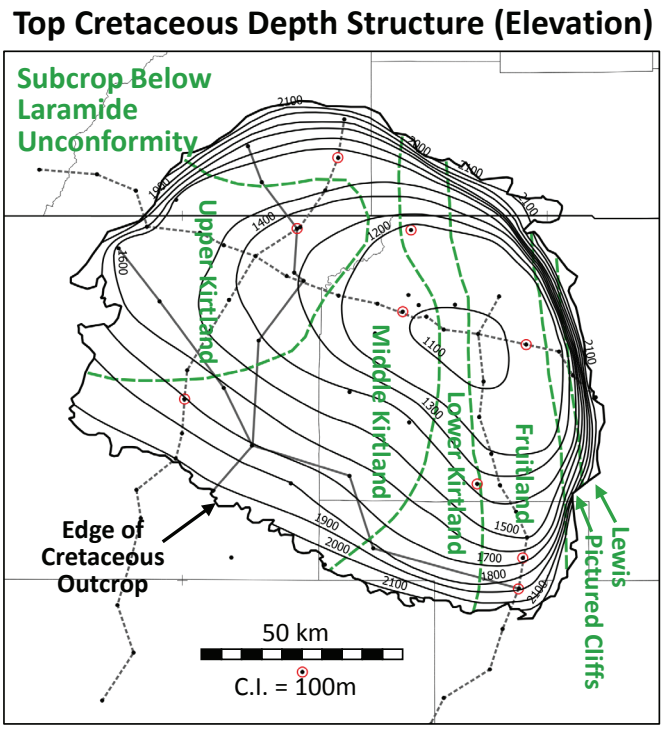

Figure 5C. Structural elevation of the top Cretaceous surface. Results are very similar to Cather (2004). In green, are subcrop belts below top Cretaceous (Laramide) unconformity. Progressively older units subcrop to the southeast.

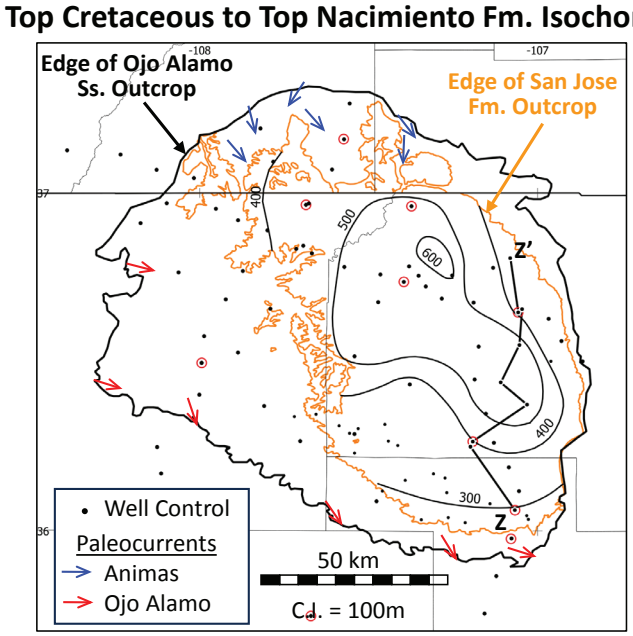

Figure 5D. Isochore of the top Cretaceous to top Nacimiento Formation (~66–55 Ma) interval. Paleocurrents are generalized from the compilation of Pecha et al. (2018). Somewhat symmetrical thickening into the basin is observed.

thermochronology to infer the exhumation history on the Nacimiento Uplift. Most samples indicated Eocene exhumation, consistent with this interpretation (Supplement 1.8).

Subsidence Phases

We interpreted six phases of subsidence/uplift based on temporal patterns of subsidence via basin models, stacking patterns, and isochore maps (Figs. 2, 3A, and 3B). Cather (2004) made somewhat similar observations using raw thickness trends (not including decompaction, changes in paleobathymetry/paleoelevation, or reconstructed section).

Phase 1, the Turonian to Santonian (~93–84 Ma), was characterized by a uniform and high rate of subsidence throughout the basin. Although somewhat diachronous, this pattern is seen throughout the U.S. Western Interior region. It has been interpreted as dynamic subsidence related to the mantle convection driven by the subducted Farallon slab and the approaching conjugate Shatsky Rise (Liu and Gurnis, 2010; Li and Aschoff, 2022).

Phase 2, the early Campanian (~84–80 Ma), had a modest decrease in subsidence that was coeval with the progradation of the Point Lookout Sandstone shoreline and associated Menefee Formation coastal plain (Molenaar, 1983; Fig. 2). We hypothesized that this major regression may have been related to a lower rate of sedimentary accommodation (subsidence) as seen on the basin modeling geohistories (Phase 2 on Figs. 3A and 3B). While an increase in sediment supply could also be a factor, this mechanism implies a more regional source, rather than local uplift. Detrital zircon analysis indicates local sourcing for Kirtland Formation and younger sediments (Pecha et al., 2018).

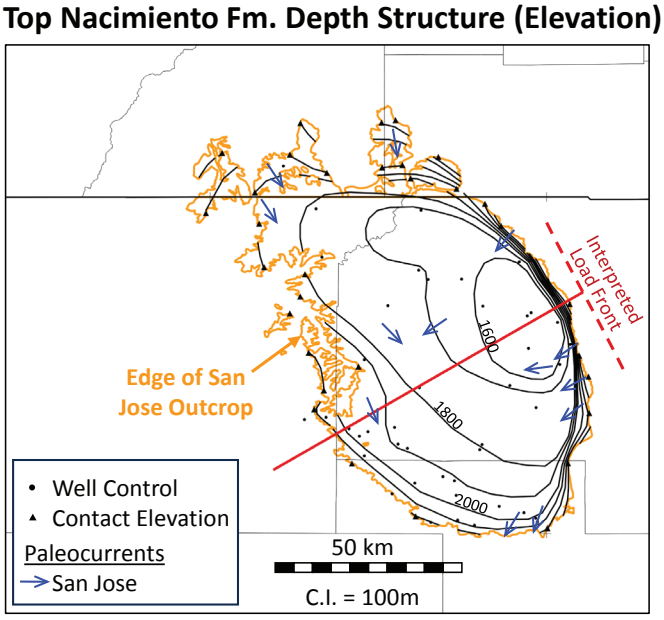

Figure 5E. Structural elevation of the top Nacimiento Formation (Paleocene) surface (~55 Ma). Control points include correlated wells, and surface elevations at the top Nacimiento Formation/base San Jose Formation contact. Paleocurrents are generalized from the compilation of Pecha et al. (2018). Very steep dips to the southwest are observed on the east flank of the basin, adjacent to the Nacimiento uplift and Archuleta arch.

At the base of Phase 3, an increase of subsidence and a commensurate transgression occurred, with the retrogradational stacking of the Lewis Shale on top of the Cliff House Sandstone (Molenaar, 1983; Fig. 2). Subsidence during this late Campanian (~80–66 Ma) stratigraphic interval was spatially variable, which is illustrated in isochore maps and basin models (Figs. 3A, 3B, and 5B). The greatest subsidence was in the northwest. This was interpreted as a flexural response to Laramide orogenic-related uplift of the Hogback monocline and western San Juan uplift. The initial period (Phase 3A) displays the highest rate of subsidence and was associated with the retrogradation from the Menefee Formation top to Lewis Shale maximum-flooding surface. Subsidence rate decreased in the Maastrichtian (Figs. 3A and 3B), coincident with the progradation of the Pictured Cliffs Sandstone shoreline and Fruitland Formation/Kirtland Formation coastal plain.

Phase 4 represents the Laramide unconformity at the top Cretaceous/base Paleocene, which has been interpreted as the period of maximum Laramide deformation (Weil and Yonkee, 2023). Based on subcrop patterns, there was broad uplift and erosion. Moreover, a basinward tilt up to the east occurred at this time, subparallel to the flexural effects of Phase 3 (Fig. 5C). Therefore, the pattern of subcrop beneath the top of Cretaceous unconformity indicates a superposition of flexurally induced tilting and longer-wavelength uplift. The fluvial Ojo Alamo Sandstone was deposited on this surface over much of the basin.

Phase 5 was a resumption of rapid subsidence in the Paleocene (Nacimiento Formation; Fig. 5D) and early Eocene (San Jose Formation). The highest interpreted subsidence in the early Eocene occurs in the northeast, adjacent to the Nacimiento uplift and Archuleta arch.

Phase 6 represents uplift and exhumation that occurred after the early Eocene. Evidence includes the outcrop pattern of progressively older strata on the flanks of the basin (Fig, 1). More importantly, calibrated basin modeling, tied to vitrinite reflectance measurements in wells, estimated 1–2 km of removed section (Supplement 2).

The timing of exhumation was addressed by numerous studies in the Western Interior, based on thermochronology, paleobotany, isotopic analysis, and vesicle paleoaltimetry, yielding variable results; a good summary can be found in Cather et al. (2012). To the southwest, in the Chuska Mountains, Cather et al. (2008) interpreted exhumation as occurring at 15 Ma, as evidenced by the thick aggradational succession of Oligocene eolianites. On the Zuni uplift to the south, Thacker et al. (2021) used AFT thermochronology to infer the exhumation history. Campanian to Eocene cooling is observed on the flanks and crest, consistent with Laramide uplift. They also observed a second exhumation event beginning ~20 Ma on the northeastern flank, generally aligned with the interpretation of Cather et al. (2008). Flowers et al. (2008) interpreted the onset of exhumation at about 28 Ma from apatite U-Th/He thermochronology.

For this study, the timing and amount of erosion (exhumation) and uplift (elevation change) had little impact on the interpretation and modeling of early Eocene and older

subsidence. An exception would be if we had evidence of post-Eocene large magnitude tilting or deformation in the basin center, which would affect the Nacimiento Formation top structure map (Fig. 5E.) We have assumed that most elevation change, and all post-Eocene exhumation, occurred after 20 Ma (Figs. 3A and 3B).

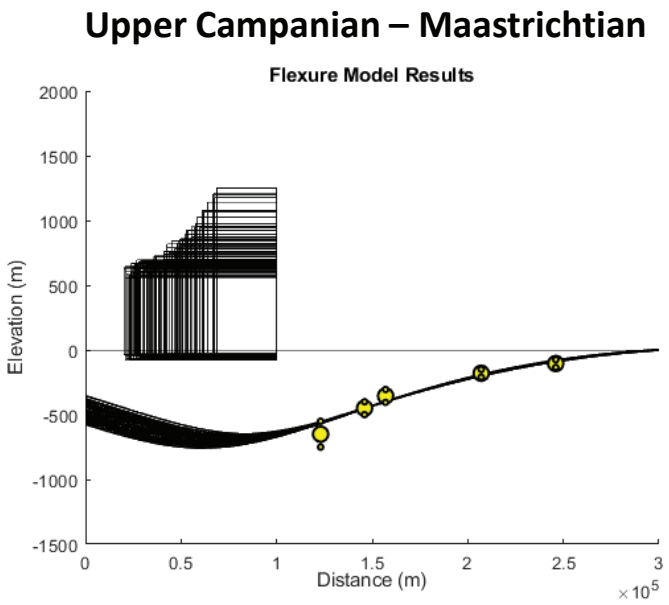

Figure 6A. Reference case flexural model for upper Campanian through Maastrichtian interval (i.e., Huerfanito Bentonite to top Cretaceous interval). The location of the stratigraphic profile is shown on Figure 5B, and the control points are the large yellow dots, and the small yellow dots illustrate the acceptable error range. The program performs a Monte Carlo simulation, varying load height, width, and effective elastic thickness (EET). Modeled profiles and associated loads that satisfy the stratigraphic control points are shown as the cloud of successful trials. The program reports the mean and standard deviation of the modeled parameters (load height, width, and EET).

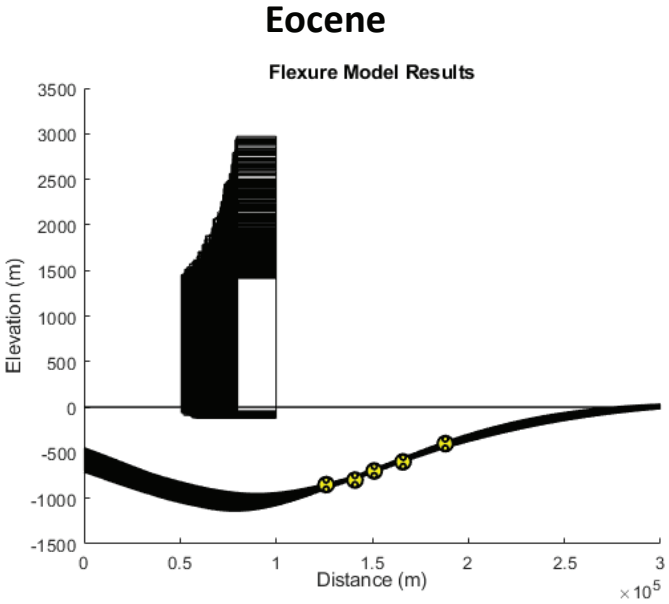

Figure 6B. Reference case flexural model for Eocene interval. See text and Figure 6A for explanation of flexural modeling characteristics.

The Oligocene was interpreted as a period of relative tectonic quiescence. Based on occurrences in the Chuska Mountains, San Juan Mountains, and Mogollon-Datil areas, there is a possibility that Oligocene eolianites and/or volcanics were emplaced in the basin (Cather et al., 2008) and subsequently eroded during Miocene to recent exhumation. No attempt has been made to reconstruct such aggradational deposits in the basin models.

Regional Patterns

The correlation between 2nd order stacking patterns and tectonic subsidence/uplift is recognized for other parts of the Western Interior region (Supplement 1.2). To the immediate north, the Uinta, Piceance, and Park basins of Utah and Colorado display a simpler large-scale stacking. First, there was an increase in subsidence near the end of the Turonian and an associated retrograde from the Ferron Sandstone and Frontier Formation into the main body of the Mancos Shale (upper Coniacian to lower Santonian). The strata became strongly progradational in the middle to upper Campanian, as the total subsidence rate decreased (Aschoff and Steel, 2011). The Campanian–Maastrichtian succession of progradation-retrogradation-progradation of the San Juan is absent here.

Farther north, stacking patterns in the Wyoming basins appear superficially similar to the San Juan Basin at first glance (Rudolph et al., 2015). A large magnitude, forced regression of the fluvial system recorded by the Ericson Sandstone, Parkman Sandstone, and Teapot Sandstone occurred during a period of decreased subsidence or uplift, analogous to the Menefee Formation. This was followed by a profound transgression marked by the Lewis Shale, which has been related to flexural subsidence associated with Laramide uplifts such as the Granite Mountains, Uinta Mountains, Big Horn Mountains, and others (Rudolph et al., 2015; Lynds and Lichtner, 2016; Saylor et al., 2020). The succession is capped by a progradational stratal stack consisting of shallow marine Fox Hills Sandstone and coastal plain Lance Formation.

Although the patterns of stratigraphic sequence stacking, tectonic activity, and subsidence appear analogous between the San Juan and Green River basins, there are two critical differences. First, the transgressive-regressive cycles observed in the San Juan Basin occurred earlier than similar cyclicity observed in Wyoming. For example, the Ericson Sandstone regression in Wyoming occurred ~79–72 Ma (Rudolph et al., 2015), whereas the Menefee Formation progradation occurred ~84–80 Ma (Fig. 2, Supplement 1.2). Furthermore, Lewis Shale maximum flooding occurred at ~72 Ma (Asquith Zone) in Wyoming, whereas the Huerfanito Bentonite maximum flood occurred at ~75.8 Ma in the San Juan Basin. This indicates that the large-scale (2nd order), transgressive-regressive cycles observed in these basins are unlikely to be eustatic in origin. Rather, their comparative diachroneity supports a tectonic driver of stratal cyclicity that was variable along strike.

The second difference is in the magnitude of loads and flexural subsidence. The Wyoming examples include many larger uplifts that commensurately induced larger flexural responses

in adjacent basins (Fig. 7). There are seven examples of modeled topographic uplifts of greater than 1 km (Saylor et al., 2020). The most notable example is the east Green River basin, which recorded deep-water deposition in the Maastrichtian with estimated paleobathymetry of 300–500 m, based on seismic clinoforms (Rudolph et al., 2015) and correlated well logs (Carvajal and Steel, 2012). In many of the Western Interior basins, the earliest documented evidence of Laramide flexure is in the Maastrichtian, whereas flexure in the San Juan Basin was interpreted to have started in the Campanian. However, other early examples (Turonian to Campanian) of Laramide uplift have been observed in Wyoming and Montana (Carrapa et al., 2019; Saylor et al., 2020).

CONCLUSIONS

San Juan Basin Upper Cretaceous to Cenozoic strata record six phases of subsidence/uplift that have different drivers based on stratigraphic thickness and stacking patterns. Subsidence from the Cenomanian to Santonian appears to be of long wavelength, which we interpreted to be associated with dynamic effects related to mantle convection, as has been posited for the Western Interior basin (Liu and Nummedal, 2004; Liu and Gurnis, 2010). Laramide orogenesis in the San Juan Basin area began by late Campanian time, with a modest uplift northwest of the basin associated with early uplift of the San Juan uplift and Hogback monocline. This deformation is observed in subcrop patterns beneath the Laramide unconformity (Fig. 5C). As a result, the onset of flexural subsidence may have contributed to the profound transgression of the Menefee Formation into the Lewis Shale maximum flooding event. Above the Huerfanito Bentonite, a strong progradational pattern into the Pictured Cliffs Sandstone (shallow marine) and Fruitland Formation and Kirtland Formation (nonmarine) was driven by a decreased subsidence rate. Flexural modeling of this episode indicated that the San Juan uplift and Hogback monocline to the northwest of the basin were the likely flexural loads and exhibited a mean topographic height of ~0.8 km.

Similar (and usually much larger) Late Cretaceous flexural effects are seen in many other Laramide basins in Wyoming and northern Colorado (Fig. 7). This includes a strong retrogradational pattern at the start of flexural subsidence.

Paleocene San Juan Basin stratigraphy (Ojo Alamo Sandstone and Nacimiento Formation) thickens toward the basin center, exhibiting a much more symmetrical pattern (Fig. 5D) than observed in Upper Cretaceous strata. This possibly represents a composite flexural effect from adjacent Laramide uplifts to the northwest, northeast, and east of the basin. Another contributing factor to the thickness pattern observed during this episode (Fig. 5D) may be infill of paleorelief via alluvial aggradation within a semienclosed basin. Note this also infers Laramide uplifts rimming the basin.

Flexural modeling of the Eocene strata of the San Juan Basin (Fig. 5E) indicated that the locus of flexural loading shifted to the east. The Nacimiento uplift and Archuleta arch provided the flexural load. This was a relatively significant uplift, with a mean topographic height of ~2 km (Fig. 6B). Furthermore, we interpreted the eastward shift of the basin depocenter to reflect continued evolution of Laramide tectonic activity within the study area.

In summary, the large-scale basin architecture and vertical stacking patterns from Campanian to Eocene were primarily driven by the timing, magnitude, and spatial distribution of Laramide uplift and associated flexural subsidence.

The wavelength of the interpreted flexural effects is relatively short. Consequently, the estimates of the flexural rigidity of the coupled lithosphere from modeling are relatively low (20–30 km) and broadly consistent with modern estimates from seismic tomography.

ACKNOWLEDGMENTS

This paper benefitted from the thorough reviews of Kevin Biddle, Steve Cather, and Jerry Kendall. Any use of trade, firm, or product names is for descriptive purposes only and does not imply endorsement by the U.S. government.

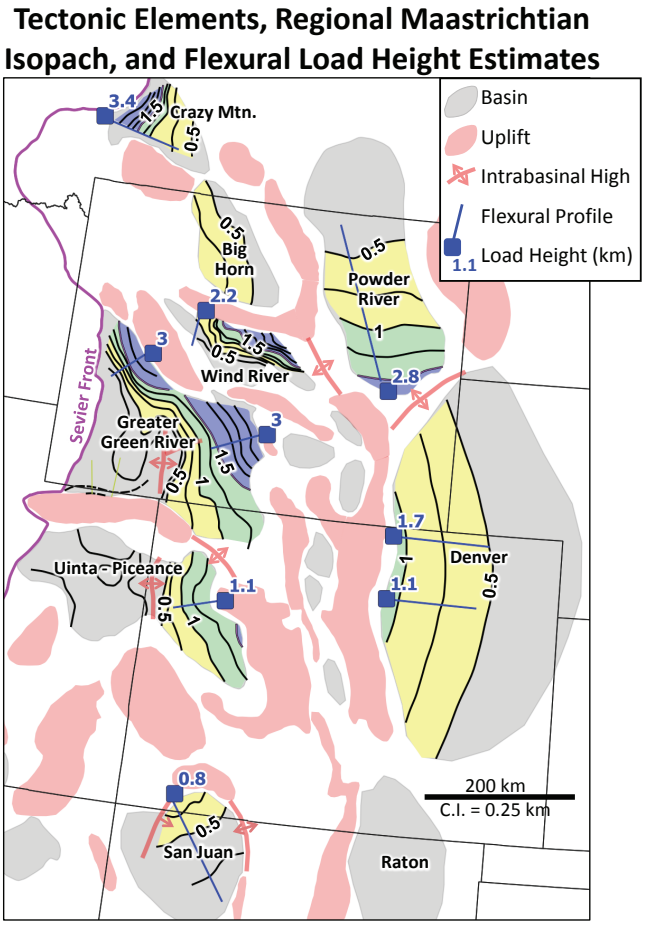

Figure 7. Regional ~Maastrichtian isochores of the Western Interior region basins, with estimates of topographic uplift from flexural modeling indicated in red. Isochore isoline labels are provided in km and shaded blue-green-yellow-gray to convey thick to thin stratal trends, respectively. Note that the San Juan Basin isopach is upper Campanian to Maastrichtian, while the others are Maastrichtian. Modified from Saylor et al. (2020). Uplifts are identified in Supplement 1.1.

REFERENCES

Aschoff, J., and Steel, R. 2011, Anomalous clastic wedge development during the Sevier-Laramide transition, North American Cordilleran foreland basin, USA: Geological Society of America Bulletin, v. 123, p. 1822–1835. https://doi.org/10.1130/B30248.1

Baltz, E.H., 1967, Stratigraphy and regional tectonic implications of part of Upper Cretaceous and Tertiary rocks, east-central San Juan Basin, New Mexico: U.S. Geological Survey Professional Paper 552, 100 p. https://doi.org/10.3133/pp552

Beaumont, C., 1981, Foreland basins: Geophysical Journal International, v. 65, p. 291–329.

Blackwell, D., Richards, M., Frone, Z., Batir, J., Ruzo, A., Dingwall, R., and Williams, M., 2011, Temperature at depth maps for the conterminous US and geothermal resource estimates, Geothermal Resources Council Transactions, v. 35, p. 1545–1550.

Bradley, W.H., 1948, Liminology and the Eocene lakes of the Rocky Mountain Region: Geological Society of America Bulletin, v. 59, p. 635–648. https://doi.org/10.1130/0016-7606(1948)59[635:LATELO]2.0.CO;2

Broadhead, R.F., Wilks, M., Morgan, M., and Johnson, R.E., 1998, The New Mexico petroleum source rock database: New Mexico Bureau of Geology and Mineral Resources, Digital Database DB2. https://geoinfo.nmt.edu/publications/databases/dds/2/home.cfm (accessed 31 January 2025).

Carrapa, B., DeCelles, P.G., and Romero, M., 2019, Early inception of the Laramide orogeny in southwestern Montana and northern Wyoming—Implications for models of flat-slab subduction: Journal of Geophysical Research—Solid Earth, v. 124, p. 2102–2123. https://doi.org/10.1029/2018JB016888

Carvajal, C.R., and R.J. Steel, 2012, Source-to-sink sediment volumes within a tectonostratigraphic model for a Laramide shelf–to–deep-water basin—Methods and results, *in* C. Busby and A. Azor, eds., Tectonics of Sedimentary Basins—Recent Advances: Oxford, United Kingdom, Wiley-Blackwell, p. 131–151.

Cather, S.M., 2003, Polyphase Laramide tectonism and sedimentation in the San Juan Basin, New Mexico: New Mexico Geological Society, Guidebook 54, p. 119–132. https://doi.org/10.56577/FFC-54.119

Cather, S.M., 2004, The Laramide orogeny in central and northern New Mexico and southern Colorado, *in* Mack, G.H., and Giles, K.A., eds., The Geology of New Mexico, A Geologic History: New Mexico Geological Society Special Publication 11, p. 203–248. https://doi.org/10.56577/SP-11.

Cather, S.M., Chapin, C.E., and Kelley, S.A., 2012, Diachronous episodes of Cenozoic erosion in southwestern North America and their relationship to surface uplift, paleoclimate, paleodrainage, and paleoaltimetry: Geosphere, v. 8, p. 1177–1206. https://doi.org/10.1130/GES00801.1

Cather, S.M., Connell, S.D., Chamberlin, R.M., McIntosh, W.C., Jones, G.E., Potochnik, A.R., Lucas, S.G., and Johnson, P.S., 2008, The Chuska erg—Paleogeomorphic and paleoclimatic implications of an Oligocene sand sea on the Colorado Plateau: Geological Society of America Bulletin, v. 120, p. 13–33. https://doi.org 10.1130/B26081.1

Cather, S.M., Heizler, M.T., and Williamson, T.E., 2019, Laramide fluvial evolution of the San Juan Basin, New Mexico and Colorado—Paleocurrent and detrital-sanidine age constraints from the Paleocene Nacimiento and Animas formations: Geosphere, v. 15, no. 5, p. 1641–1664. https://doi.org/10.1130/GES02072.1

Chapin, C.E. and Cather, S.M., 1983, Eocene paleotectonics and sedimentation in the Colorado Plateau Rocky Mountain area: American Association of Petroleum Geologists Bulletin, v. 67, no. 8, p. 1331–1332. https://doi.org/10.1306/03B5B7FE-16D1-11D7-8645000102C1865D

Chapman, J.B., and DeCelles, P.G., 2021, Beveling the Colorado Plateau—Early Mesozoic rift-related flexure explains erosion and anomalous deposition in the southern Cordilleran foreland basin: Tectonics, v. 40, no. 6. https://doi.org/10.1029/2020TC006517

Colorado Energy and Carbon Management Commission, 2025, Imaged document search tool: https://ecmc.state.co.us/weblink/ (accessed 15 January 2025).

Coney, P.J., 1971, Cordilleran tectonic transitions and motion of the North American plate: Nature, v. 233, p. 462–465. https://doi.org/10.1038/233462a0

Copeland, P., Currie, C.A., Lawton, T.F., and Murphy, M.A., 2017, Location, location, location—The variable lifespan of the Laramide orogeny: Geology, v. 45, no. 3, p. 223–226. https://doi.org/10.1130/G38810.1

Davis, G.H., Reeher, L.J., Jepson, G., Carrapa, B, DeCelles, P.G., and Chaudoir, K.M., 2022, Structure and thermochronology of basement/cover relations along the Defiance Uplift (AZ and NM), and implications regarding Laramide tectonic evolution of the Colorado Plateau: American Journal of Science, v. 322, p. 1047–1087. https://doi 10.2475/09.2022.02

Decelles, P.G., 2004, Late Jurassic to Eocene evolution of the Cordilleran thrust belt and foreland basin system, western USA: American Journal of Science, v. 304, p. 105–168. https://doi.org/10.2475/ajs.304.2.105

DeCelles, P.G., and Giles, K.A., 1996, Foreland basin systems: Basin Research, v. 8, p. 105–123. https://doi.org/10.1046/j.1365-2117.1996.01491.x

Dickinson, W.R., Klute, M.A., Hayes, M.J., Janecke, S.U., Lundin, E.R., McKittrick, M.A., and Olivares, M.D., 1988, Paleogeographic and paleotectonic setting of Laramide sedimentary basins in the central Rocky Mountain region: Geological Society of America Bulletin, v. 100, p. 1023–1039. https://doi.org/10.1130/0016-7606(1988)100<1023:PAPSOL>2.3.CO;2

DuBois, D.P., Wynne, P.J., Smagala, T.M., Johnson, J.L., Engler, K.D., and McBride, B.C., 2004, Geology of Jonah field, Sublette County, Wyoming, *in* Robinson, J.W. and Shanley, K.W., eds., Jonah Field—Case Study of a Giant Tight-Gas Fluvial Reservoir: American Association of Petroleum Geologists Studies in Geology 52 and Rocky Mountain Association of Geologists 2004 Guidebook, p. 37–59. https://doi.org/10.1306/St521007

Fassett, J.E., 1991, Oil and gas resources of the San Juan Basin, New Mexico and Colorado, *in* Gluskoter, H.J., Rice, D.D., and Taylor, R.B., eds., Economic Geology: Geological Society of America, The Geology of North America Series, v. P-2, p. 357–372.

Fassett, J.E., 2000, Geology and coal resources of the Upper Cretaceous Fruitland Formation, San Juan Basin, New Mexico and Colorado, *in* Kirschbaum, M.A., Roberts, L.N.R., and Biewick, L.R.H., eds., Geologic assessment of coal in the Colorado Plateau: Arizona, Colorado, New Mexico, and Utah: U.S. Geological Survey Professional Paper 1625–B, p. Q1–Q132.

Fassett, J.E., Cobban, W.A., and Obradovich, J.D., 1997, Biostratigraphic and isotopic age of the Huerfanito bentonite bed of the upper Cretaceous Lewis Shale at an outcrop near Regina, New Mexico: New Mexico Geological Society, Guidebook 48, p. 229–242. https://doi.org/10.56577/FFC-48.229

Fassett, J.E., and Nucio, V.F., 1990, Vitrinite reflectance values of coal from drill-hole cuttings from the Fruitland and Menefee Formations, San Juan Basin, New Mexico: U.S. Geological Survey Open-File Report 90-290, 21 p.

Feldman, H.R., Fabijanic, J.M., Faulkner, B.L., and Rudolph, K.W., 2014, Lithofacies, parasequence stacking, and depositional architecture of wave to tide-dominated shorelines in the Frontier Formation, western Wyoming, U.S.A.: Journal of Sedimentary Research, 2014, v. 84, p. 694–717. https://dx.doi.org/10.2110/jsr.2014.53

Flowers, R.M., Wernicke, B.P., and Farley, K.A., 2008, Unroofing, incision, and uplift history of the southwestern Colorado Plateau from apatite (U-Th)/He thermochronometry: Geological Society of America Bulletin, v. 120, p. 571–587. https://doi.org/10.1130/B26231.1

Gao, M., and Fan, M., 2018, Depositional environment, sediment provenance and oxygen isotope paleoaltimetry of the early Paleogene Greater Green River Basin, southwestern Wyoming, U.S.A.: American Journal of Science, v. 318, p. 1018–1055. https://doi.org/0.2475/10.2018.02

Gradstein, F.G., Ogg, J.G., Schmitz, M.D., and Ogg, G.M., eds., 2020, Geologic Time Scale 2020: Amsterdam, Elsevier, 240 p.

Hagen, S.E., Shuster, M.W., and Furlong, K.P., 1985, Tectonic loading and subsidence of intermontane basins—Wyoming foreland province: Geology, v. 13, p. 585–588. https://doi.org/10.1130/0091-7613(1985)13<585:TLASOI>2.0.CO;2

Hantschal, T., and Kauerauf, A.I., 2009, Fundamentals of Basin and Petroleum Systems Modeling: Berlin Heidelberg, Springer-Verlag, 476 p. https://doi.org/10.1007/978-3-540-72318-9

Helland-Hansen, W., and Martinsen, O.J., 1996, Shoreline trajectories and sequences—Description of variable depositional-dip scenarios: Journal of Sedimentary Research, Section B—Stratigraphy and Global Studies, v. 66, no. 4, p. 670–688. https://doi.org/10.1306/D42683DD-2B26-11D7-8648000102C1865D

Horton, J.D., 2017, The state geologic map compilation (SGMC) geodatabase of the conterminous United States (ver. 1.1, August 2017): U.S. Geological Survey Data Release. https://doi.org/10.5066/F7WH2N65

Horton, B., Capaldi, T., Mackaman-Lofland, C., Perez, N., Bush, M., Fuentes, F., and Constenius, K., 2022, Broken foreland basins and the influence of subduction dynamics, tectonic inheritance, and mechanical triggers: Earth-Science Reviews, v. 234, p. 1–28. https://doi.org/10.1016/j.earscirev.2022.104193

Houseknecht, D.W., 2019, Petroleum systems framework of significant new oil discoveries in a giant Cretaceous (Aptian–Cenomanian) clinothem in Arctic Alaska: American Association of Petroleum Geologists Bulletin, v. 103, p. 619–652. https://doi/10.1306/08151817281

Kluth, C.F., 1986, Plate tectonics of the Ancestral Rocky Mountains, *in* Peterson, J.A., ed., Paloetectonics and Sedimentation in the Rocky Mountain Region, United States: American Association of Petroleum Geologists Memoir 41, p. 353–369.

Kelley, S.A., Chapin, C.E., and Corrigan, J., 1992, Late Mesozoic to Cenozoic cooling histories of the flanks of the northern and central Rio Grande rift, Colorado and New Mexico: New Mexico Bureau of Mines and Mineral Resources, Bulletin 145, 40 p. https://doi.org/10.58799/B-145

Law, B.E., 1990, Vitrinite reflectance data from Cretaceous and Tertiary Rocks, San Juan Basin, New Mexico and Colorado: U.S. Geological Survey Open-File Report 90-659, 18 p.

Law, B.E., 1992, Thermal maturity patterns of Cretaceous and Tertiary rocks, San Juan Basin, Colorado and New Mexico: Geological Society of America Bulletin, v. 104, p. 192–207. https://doi.org/10.1130/0016-7606(1992)104<0192:TMPOCA>2.3.CO;2

Leary, R.J., Umhoefer, P., Smith, M.E., and Riggs, N., 2017, A three-sided orogen—A new tectonic model for Ancestral Rocky Mountain uplift and basin development: Geology, v. 45, no. 8, p. 735–738. http://doi.org/10.1130/abs/2016AM-280369

Li, Z., and Aschoff, J., 2022, Constraining the effects of dynamic topography on the development of Late Cretaceous Cordilleran foreland basin, western United States: Geological Society of America Bulletin, v. 134, p. 446–462. https://doi.org/10.1130/B35838.1

Lipman, P.W., Prostka, H.J., and Christiansen, R.L., 1972, Evolving subduction zones in the western United States: Science, v. 174, p. 821–825. https://doi.org/10.1126/science.174.4011.821

Liu, L., and Gurnis, M., 2010, Dynamic subsidence and uplift of the Colorado Plateau: Geology, v. 38, no. 7, p. 663–666. https://doi.org/10.1130/G30624.1

Liu, S., and Nummedal, D., 2004, Late Cretaceous subsidence in Wyoming—Quantifying the dynamic component: Geology, v. 32, no. 5, p. 397–400. https://doi.org/10.1130/g20318.1

Lynds, R.M., and Lichtner, D.T., 2016, Stratigraphy and hydrocarbon potential of the Fort Union and Lance Formations in the Great Divide and Washakie Basins, South-Central Wyoming: Wyoming State Geological Survey Report of Investigations 73, 70 p.

McIntosh, W.C., Chapin, C.E., Ratte, J.C., Sutter, J.F., 1992, Time-stratigraphic framework for the Eocene–Oligocene Mogollon-Datil volcanic field, southwest New Mexico: Geological Society of America Bulletin, v. 104, p. 851–871. https://doi.org/10.1130/0016-7606(1992)104<0851:TSFFTE>2.3.CO;2

Merewether, E.A. and McKinney, K.C., 2015, Composite biostratigraphic outcrop sections for Cretaceous formations along a south-trending transect from northwestern Montana to northwestern New Mexico: U.S. Geological Survey Open-File Report 2015–1087.

Molenaar, C.M., 1977, San Juan Basin time-stratigraphic nomenclature chart: New Mexico Geological Society, Guidebook 28, p. xii. https://doi.org/10.56577/FFC-28.xii

Molenaar, C.M., 1983, Major depositional cycles and regional correlations of Upper Cretaceous rocks, southern Colorado Plateau and adjacent areas, *in* Reynolds, M.W., and Dolly, E.D., eds., Mesozoic Paleogeography of the West-Central United States: Rocky Mountain Section, SEPM (Society for Sedimentary Geology) Rocky Mountain Paleogeography Symposium 2, p. 201–224.

Molenaar, C.M., and Baird, J.K., 1992, Regional stratigraphic cross sections of Upper Cretaceous rocks across the San Juan Basin, northwestern New Mexico and southeastern Colorado: U.S. Geological Survey Open File Report 92-257.

New Mexico Energy Minerals and Natural Resources Department, 2025, OCD online—Imaging: https://www.emnrd.nm.gov/ocd/ocd-data/ocd-imaging/ (accessed 15 January 2025).

Pawlewicz, M.J., Nuccio, V.F., and Fassett, J.E., 1991, Vitrinite reflectance values of coal from drill-hole cuttings, San Juan Basin, New Mexico: U.S. Geological Survey Open-File Report 91-302, 10 p.

Pecha, M.E., Gehrels, G.E., Karlstrom, K.E., Dickinson, W.R., Donahue, M.S., Gonzales, D.A., and Blum, M.D., 2018, Provenance of Cretaceous through Eocene strata of the Four Corners region—Insights from detrital zircons in the San Juan Basin, New Mexico and Colorado: Geosphere, v. 14, no. 2, p. 785–811. https://doi:10.1130/GES01485.1

Rudolph, K., 2023, The Ancestral Rocky Mountain Orogeny and evolution of the Permian Basin: New Mexico Geological Society, Guidebook 73, p. 147–164. https://doi.org/10.56577/FFC-73.68

Rudolph, K.W., Devlin, W.J., and Crabaugh, J.P., 2015, Upper Cretaceous sequence stratigraphy of the Rock Springs uplift, Wyoming: The Mountain Geologist, v. 52, no. 3, p. 13–157. https://doi.org/10.31582/rmag.mg.52.3.13

Russell, J.A., 1979, Vitrinite reflectance and kerogen analyses of the Great Western Drilling Co. No. 1 Hospah-Santa Fe (Mckinley County), Continental Oil Company No. 1 South Dulce (Rio Arriba County), El Paso Natural Gas Company No. 50 San Juan Unit 29-5 (Rio Arriba County), and Pan American Petroleum Corporation No. 1 Pagosa Jicarrilla (Rio Arriba County) wells, New Mexico: New Mexico Bureau of Mines and Mineral Resources, Open-File Report No. OF-265. https://doi.org/10.58799/OFR-265

Saylor, J.E., Rudolph, K.W., Sundell, K.E., and van Wijk, J., 2020, Laramide orogenesis driven by Late Cretaceous weakening of the North American lithosphere: Journal of Geophysical Research—Solid Earth, v. 125, e2020JB019570. https://doi.org/10.1029/2020JB019570

Saylor, J.E., Jordan, J.C., Sundell, K.E., Wang, X., Wang, S., and Deng, T., 2017, Topographic growth of the Jishi Shan and its impact on basin and hydrology evolution, NE Tibetan Plateau: Basin Research, v. 30, no. 3, p. 544–563. https://doi.org/10.1111/bre.12264

Tesauro, M., Kaban, M.K., Mooney, W.D., and Cloetingh, S.A.P.L., 2014, Density, temperature, and composition of the North American lithosphere—New insights from a joint analysis of seismic, gravity, and mineral physics data—2. Thermal and compositional model of the upper mantle: Geochemistry, Geophysics, Geosystems, v. 15, p. 4808–4830. https://doi.org/10.1002/2014GC005484

Tesauro, M., Kaban, M.K., and Mooney, W.D., 2015, Variations of the lithospheric strength and elastic thickness in North America: Geochemistry, Geophysics, Geosystems, v. 16, p. 2197–2220. https://doi.org/10.1002/2015GC005937

Thacker, J.O., Kelley, S.A., and Karlstrom, K.E., 2021, Late Cretaceous–Recent low-temperature cooling history and tectonic analysis of the Zuni Mountains, west-central New Mexico: Tectonics, v. 40, e2020TC006643. https://doi.org/10.1029/2020TC006643

U.S. Geological Survey, 2021, The National Map Download Application: https://apps.nationalmap.gov/downloader/ (accessed 15 January 2025).

Wangen, M., 2010, Physical principles of sedimentary basin analysis: Cambridge, Cambridge University Press, 527 p. https://doi.org/10.1017/CBO9780511711824

Watts, A.B., Ryan, W.B.F., 1976, Flexure of the lithosphere and continental margin basins: Tectonophysics, v. 36 no. 1–3, p. 25–44. https://doi:10.1016/0040-1951(76)90004-4

Weil, A.B., and Yonkee, W.A., 2012, Layer-parallel shortening across the Sevier fold-thrust belt and Laramide foreland of Wyoming—Spatial and temporal evolution of a complex geodynamic system: Earth and Planetary Science Letters, v. 357–358, p. 405–420. http://dx.doi.org/10.1016/j.epsl.2012.09.021

Weil, A.B., and Yonkee, A., 2023, The Laramide orogeny—Current understanding of the structural style, timing, and spatial distribution of the classic foreland thick-skinned tectonic system, *in* Whitmeyer, S.J., Williams, M.L., Kellett, D.A., and Tikoff, B., eds., Laurentia—Turning Points in the Evolution of a Continent: Geological Society of America Memoir 220, p. 707–771. https://doi.org/10.1130/2022.1220(33)

Williamson, T.E. and Lucas, S.G., 1992, Stratigraphy and mammalian biostratigraphy of the Paleocene Nacimiento Formation, southern San Juan Basin: New Mexico Geological Society, Guidebook 43, p. 265–296. https://doi.org/10.56577/FFC-43.265

Yonkee, W.A., and Weil, A.B., 2015, Tectonic evolution of the Sevier and Laramide belts within the North American Cordillera orogenic system: Earth-Science Reviews, v. 150, p. 531–593. https://dx.doi.org/10.1016/j.earscirev.2015.08.001

Zellman, K.L., Plink-Björklund, P., and Spangler, L., 2024, Progradational-to-retrogradational styles of Palaeogene fluvial fan successions in the San Juan Basin, New Mexico: Basin Research, v. 36, no. 1. https://doi.org/10.1111/bre.12823

Zhu, L., Fan, M., Hough, B., and Li, L., 2018, Spatiotemporal distribution of river water stable isotope compositions and variability of lapse rate in the central Rocky Mountains—Controlling factors and implications for paleoelevation reconstruction: Earth and Planetary Science Letters, v. 496, p. 215–226. https://doi.org/10.1016/j.epsl.2018.05.047

Appendices can be found at
https://nmgs.nmt.edu/repository/index.cfml?rid=2025002

Remnants of a stone building at the La Ventana mines.